ELECTRONIC SUPPLEMENTARY INFORMATION (ESI)

Shear rate dependent margination of sphere-like, oblate-like and prolate-like micro-particles within blood flow

Huilin Ye

Department of Mechanical Engineering, University of Connecticut, Storrs, CT 06269, USA.

Zhiqiang Shen

Department of Mechanical Engineering, University of Connecticut, Storrs, CT 06269, USA.

Ying Li

Department of Mechanical Engineering and Institute of Materials Science, University of Connecticut, Storrs, CT 06269, USA.

E-mail: yingli@engr.uconn.edu

1. Parameters in coarsed-grained model

Parameters	Simulation	Physical
RBC diameter (D_0)	32.0	$8 \times 10^{-6}\ m$
RBC shear modulus (μ_r)	0.01	$6.3 \times 10^{-6}\ N/m$
Energy scale ($k_{\mathrm{B}}T$)	1.1×10^{-4}	$4.14 \times 10^{-21}\ N \cdot m$
Viscosity of fluid (η)	0.167	$0.0012\ Pa \cdot s$
Area constant (k_a)	0.0075	$4.72 \times 10^{-6}\ N/m$
Local area constant (k_d)	0.367	$2.31 \times 10^{-4}\ N/m$
Volume constant (k_v)	0.096	$249\ N/m^2$
RBC bending constant (k_b)	0.013	$5 \times 10^{-19}\ N \cdot m$
MP diameter (sphere D_0)	4.0	$1 \times 10^{-6}\ m$
MP shear modulus (μ_r)	1.0	$6.3 \times 10^{-4}\ N/m$
MP area constant (k_a)	0.075	$4.72 \times 10^{-5}\ N/m$
MP local area constant (k_d)	3.67	$2.31 \times 10^{-3}\ N/m$
MP Volume constant (k_v)	0.96	$2490\ N/m^2$
MP bending constant (k_b)	0.13	$5 \times 10^{-18}\ N \cdot m$
Morse energy well width (β)	0.96	3.84 μm^{-1}
Equilibrium distance (r_0)	2.0	0.5 μm
Morse cutoff distance (r_c)	6.0	1.5 μm
LJ depth of well (ϵ)	1.1×10^{-4}	$4.14 \times 10^{-21}\ N \cdot m$
LJ zero potential distance (σ)	2.0	0.5 μm
LJ cutoff distance (r_{LJ})	2.24	0.56 μm

Table S1: Coarse-grained potential parameters, including red blood cells and MPs, and their corresponding physical values.

In the simulation, due to the numerical stability, we consider elastic MPs with high stiffness as rigid MPs. As shown in Table. S1, the MP area, local area, volume and bending constants are one order higher than those of RBC. Additionally, the shear modulus is increased by two order higher. To ensure the rigid body of MP, we impose about 2% volume expansion to the initial state of the MPs. Then there are strong volume constrains to restrict the deformation of MPs in the shear flow.

2. Quantification of margination probability

In the main text, we give the calculation method for margination probability of sphere MP as an example. Here, we illustrate this method is also valid for other types of MPs. As shown in Fig. S1, we give the calculation process of margination probability of rod MP. In the Fig. S1(a), the evolution of margination probabilities are presented for the cases with shear rate $500\ s^{-1}$ and $1000\ s^{-1}$. As we mentioned in the main text, the choice of integration interval

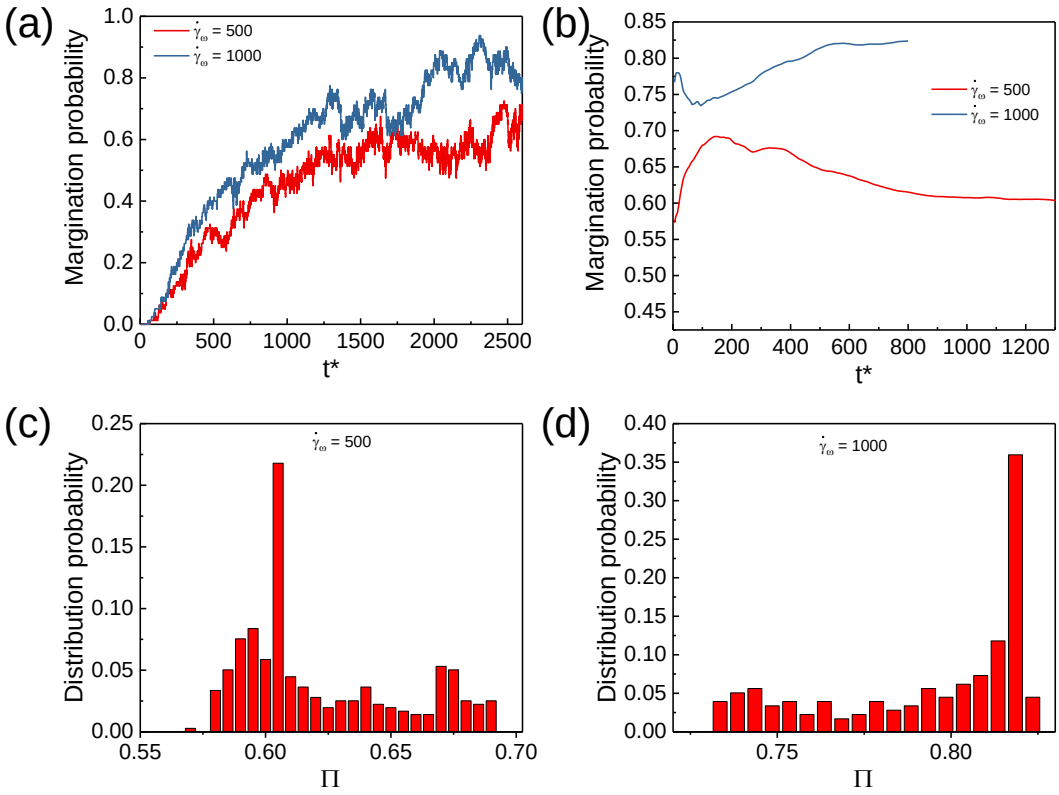

Figure S1: Calculation of the margination probability for rod MP under wall shear rates $500\ s^{-1}$ and $1000\ s^{-1}$. (a) Evolution of the margination probability. (b) Relationship between the averaged margination probability and the integration interval. (c) and (d) are the distribution of the averaged probability at wall shear rates $500\ s^{-1}$ and $1000\ s^{-1}$ respectively.

T is crucial for the calculation of margination probability. We can see that under shear rate $\dot{\gamma}_\omega = 1000s^{-1}$, when $t^* > 2000$, the probability reaches a plateau. And before that, there is large fluctuation. So, as for the case with $\dot{\gamma}_\omega = 1000s^{-1}$, T should be no more than 800 as shown in the Fig. S1(b). Then we can calculate the distribution of the margination probability and choose the most possible value as the ultimate averaged margination probability.

The integration T is determined by the steady state. We perform in totally 2700 dimensionless time, if the margination reaches steady state faster, T will be larger. For example, in the main text, for the sphere MP, we choose T as 1000. But T for the rod particles is about 600 under shear rate 1000 s^{-1} as shown in Fig. S1(b). The integration T for all cases are firstly set to 1500. And then we choose the cut-off point as final T where the margination probability enters decreasing state after steady state. The cut-off point is different for all the cases. Fig. S2 is an example for the sphere under shear rate 500 s^{-1}.

To ensure that the margination behavior of MPs reaches the steady-state regime, we run the simulation for a longer time. In the Fig. S3, we extend the simulation time to about 3500 which is about 800 longer than that in the main text. We can find that, although there still exist fluctuations of the margination probability, the change of margination probability is negligible during this extended simulation time frame. This further confirms that our simulation is long

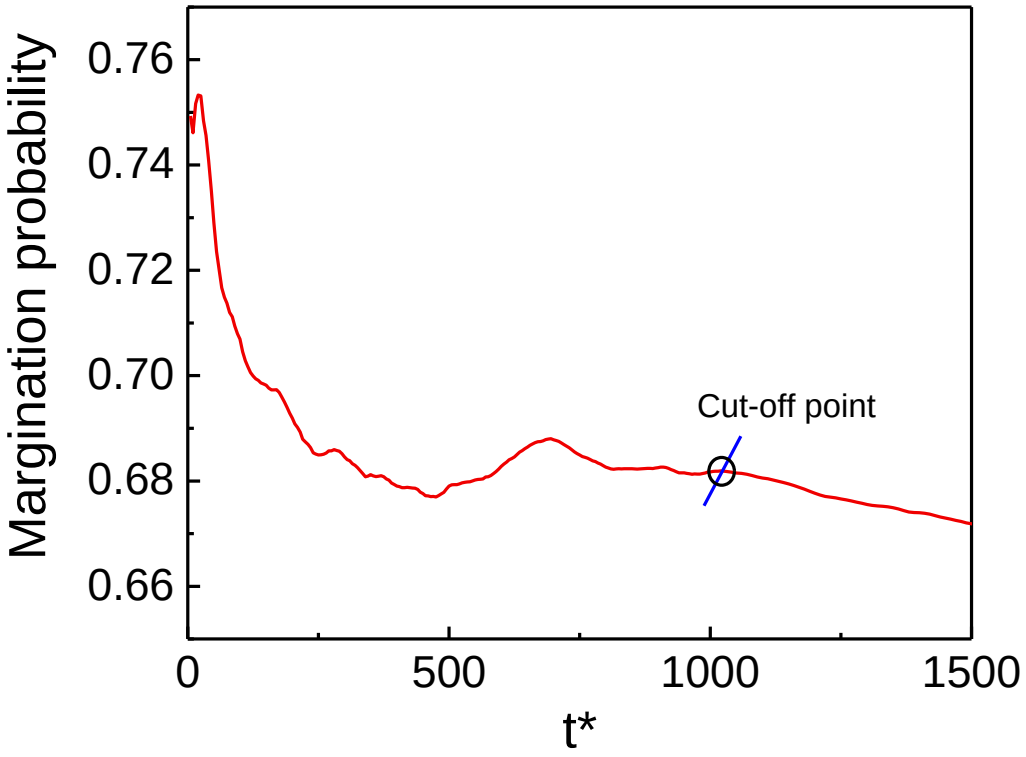

Figure S2: Determination of T: sphere MP under $\dot{\gamma}_{\omega} = 500s^{-1}$

enough for the margination behavior of MPs to reach an equilibrium state.

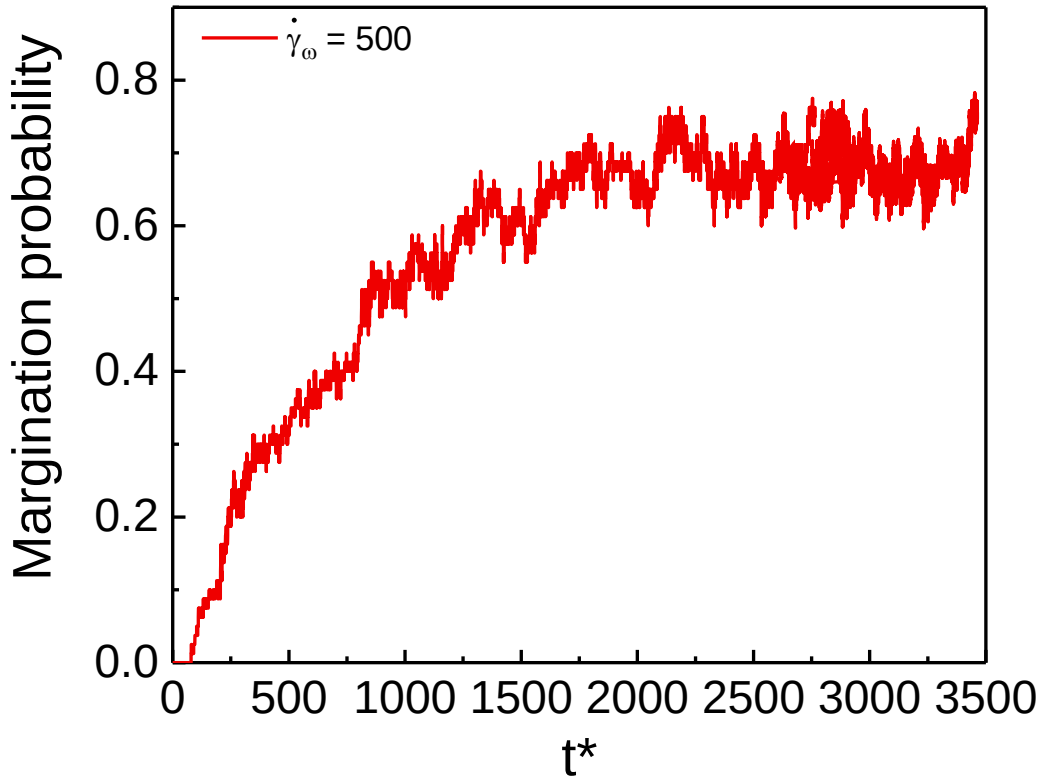

Figure S3: Evolution of margination probability of sphere MP under $\dot{\gamma}_\omega = 500s^{-1}$ for a longer simulation time.

3. Margination of MPs without RBCs in the channel

To confirm that the margination of MPs is attributed to the interaction between RBCs and MPs, we remove the RBCs in the channel and monitor the migration of MPs. All of the simulation set-ups are the same with the main text. From Fig. S4, we find that under low wall shear rate ($\dot{\gamma}_\omega <= 500s^{-1}$), the margination behavior is observed. Further increment of $\dot{\gamma}_\omega$ leads to small margination. Even for the highest $\dot{\gamma}_\omega = 2000s^{-1}$ we consider here, the margination probability is only 0.075. It reveals that the margination of MPs in the main text is mainly contributed by the interaction between RBCs and MPs. The small margination of MPs without RBCs may induced by the shear gradient of the Poiseuille flow. Although previous study [1] confirmed that a single sphere particle will reach an equilibrium place between the center of channel and wall in Poiseuille flow, here together with the interaction between spheres (80 spheres in current simulation), sphere may migrate to the near-wall region.

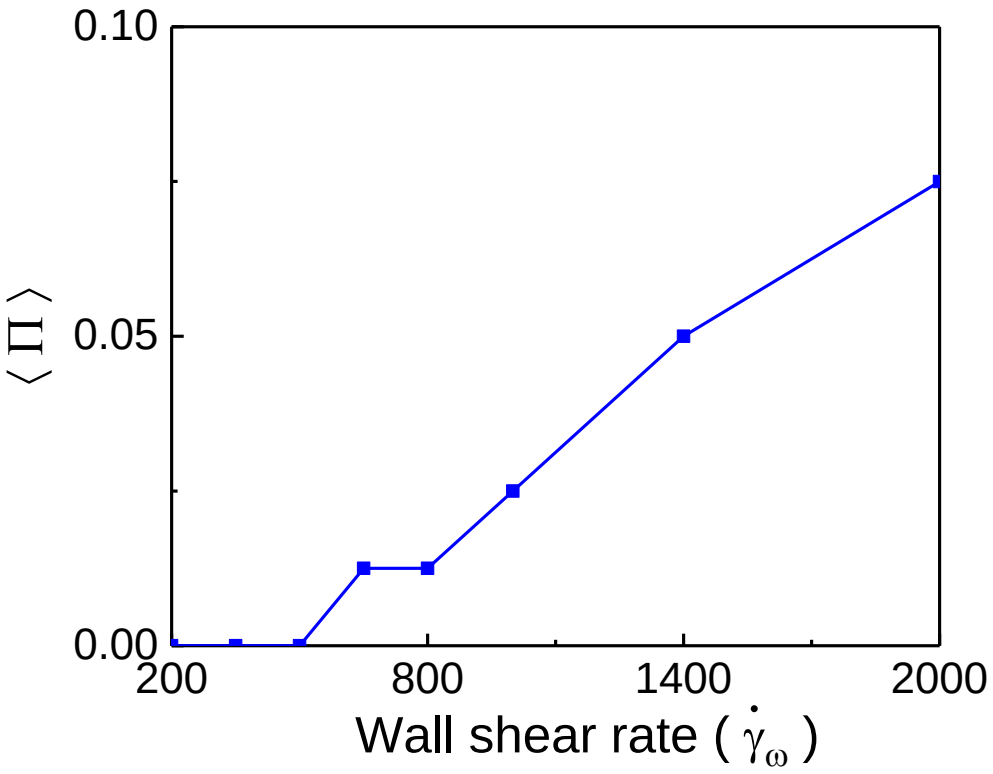

Figure S4: Margination of sphere MPs without RBCs in the channel.

4. Diffusion of MPs without RBCs

We examine the mean-squared displacement (MSD) of MPs without RBCs in the flow. The result is shown in Fig. S5, We find that the difference of diffusion among the MPs under different shear rates is not obvious. And We extract the diffusivity $D =< \Delta z^2 > /2t$. It is $3.8 \times 10^{-9} cm^{-2} s^{-1}$, which is about 12 times larger than that with RBCs in the flow. It demonstrates that the existence of RBCs indeed augments the diffusion behavior of MPs in the flow.

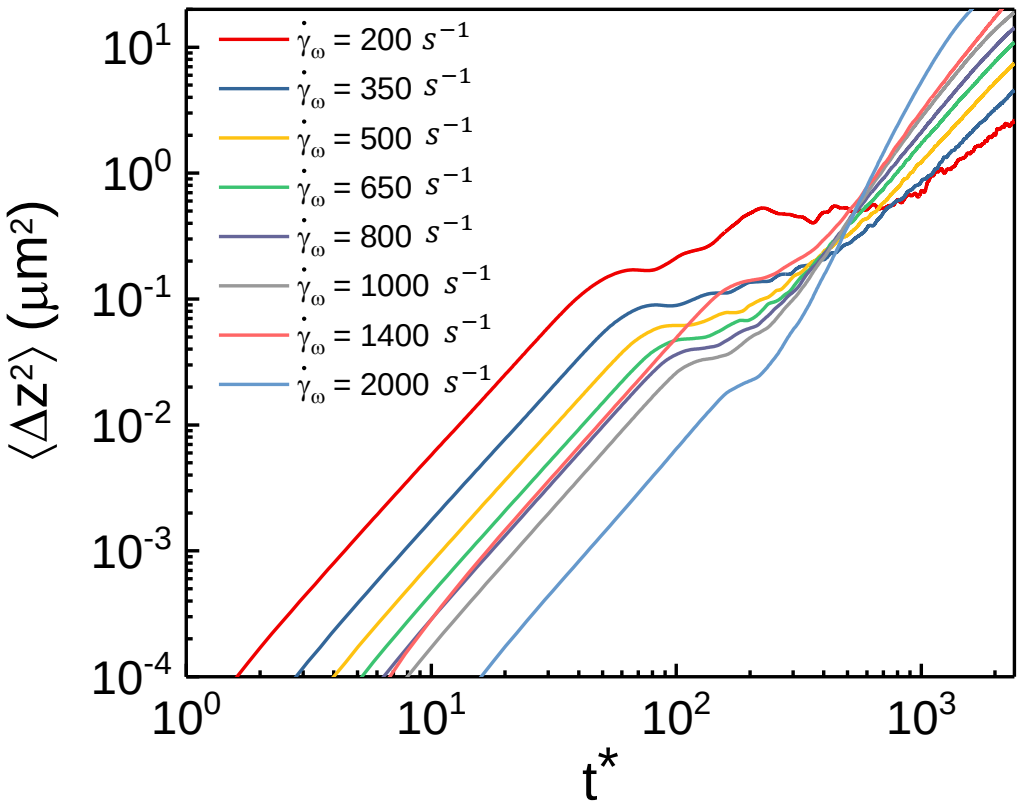

Figure S5: Mean-squared displacement of MPs without RBCs in the flow.

5. Scaling of margination probability and collision frequency for sphere MP

We find that the collision frequency of sphere MP has the same trend as the margination probability against the shear rate. We show the relationship of collision frequency with margination probability under different shear rates in the Fig. S6. We find that the relationship is approximate linear, and we fit the data using a straight line. This means that for the margination of sphere MP, the collision frequency dominates the margination behavior. Furthermore, the shear rate can affect the structure of RBCs, and structure of RBCs is associated with the collision frequency. We conclude that the shear rate is the major factor to influence the margination of sphere MP with given size.

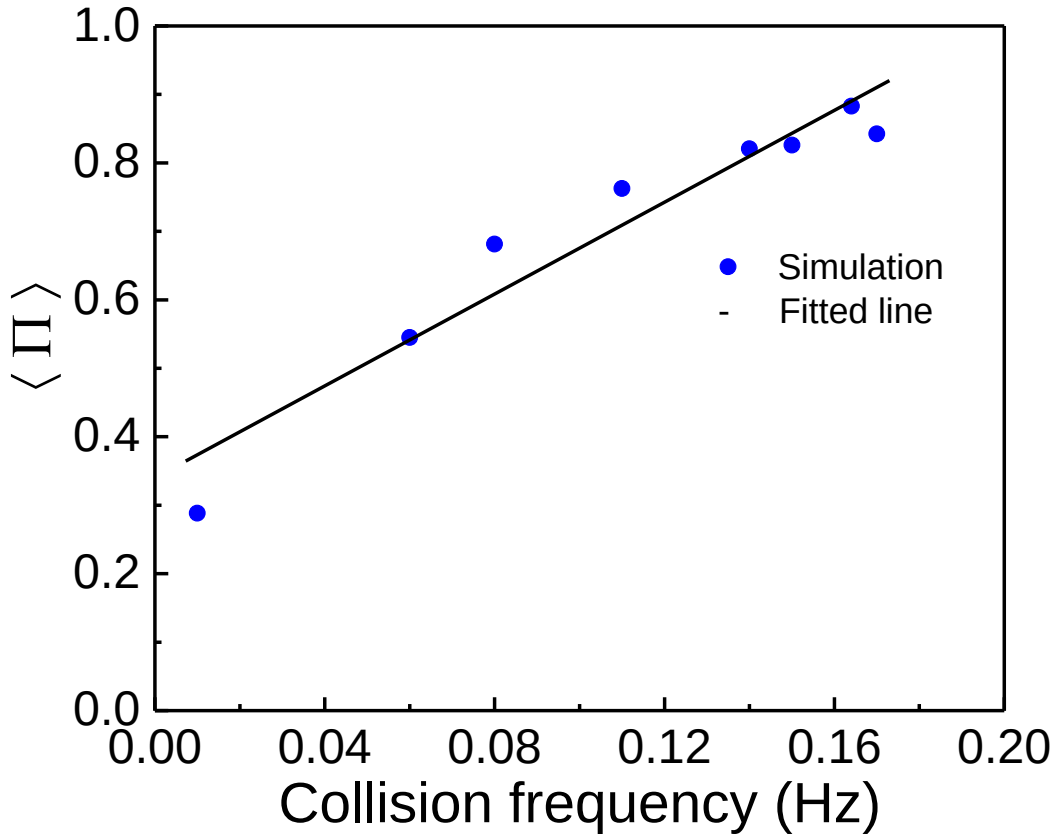

Figure S6: Scaling of margination probability and collision frequency for sphere MP under different shear rates.

References

[1] LG Leal. Particle motions in a viscous fluid. *Annual Review of Fluid Mechanics*, 12(1):435–476, 1980.